

Interstellar C_{60}^+

O. Berné^{1,2}, G. Mulas³ and C. Joblin^{1,2}

¹ Université de Toulouse; UPS-OMP; IRAP; Toulouse, France

² CNRS; IRAP; 9 Av. colonel Roche, BP 44346, F-31028 Toulouse cedex 4, France

³ Istituto Nazionale di Astrofisica – Osservatorio Astronomico di Cagliari – strada 54, localit Poggio dei Pini, 09012– Capoterra (CA), Italy

Received August ??, 2012; accepted ??, 2012

ABSTRACT

Buckminsterfullerene (C_{60}) has recently been detected through its infrared emission bands in the interstellar medium (ISM), including in the proximity of massive stars, where physical conditions could favor the formation of the cationic form, C_{60}^+ . In addition, C_{60}^+ was proposed as the carrier of two diffuse interstellar bands in the near-IR, although a firm identification still awaits gas-phase spectroscopic data. We examined in detail the *Spitzer* IRS spectra of the NGC 7023 reflection nebula, at a position close (7.5'') to the illuminating B star HD 200775, and found four previously unreported bands at 6.4, 7.1, 8.2, and 10.5 μm , in addition to the classical bands attributed to polycyclic aromatic hydrocarbons (PAHs) and neutral C_{60} . These 4 bands are observed only in this region of the nebula, while C_{60} emission is still present slightly farther away from the star, and PAH emission even farther away. Based on this observation, on theoretical calculations we perform, and on laboratory studies, we attribute these bands to C_{60}^+ . The detection of C_{60}^+ confirms the idea that large carbon molecules exist in the gas phase in these environments. In addition, the relative variation in the C_{60} and C_{60}^+ band intensities constitutes a potentially powerful probe of the physical conditions in highly UV-irradiated regions.

1. Introduction

The mid-infrared (mid-IR) spectrum of galactic and extragalactic objects exhibits band emission (strongest at 3.3, 6.2, 7.7, 8.6, and 11.2 μm) attributed to carbonaceous macromolecules, i.e., polycyclic aromatic hydrocarbons (PAHs, see recent state of the art in Joblin & Tielens 2011). In addition to PAH bands, IR emission bands at 7.0, 8.5, 17.4, and 19.0 μm have recently been reported (Cami et al. 2010; Sellgren et al. 2010), and found to match quite closely the IR active bands of buckminsterfullerene (C_{60} , Kroto et al. 1985), a cage-like carbon molecule. Carbonaceous macromolecules, including PAHs, carbon clusters, or fullerenes, are believed to play a fundamental role in the physics and chemistry of the interstellar medium (ISM), and their infrared signatures are commonly used as a tracer of physical conditions. Nevertheless, C_{60} is the only molecule belonging to this family, which has been specifically identified in the ISM. In the NGC 7023 reflection nebula, Sellgren et al. (2010) have shown that C_{60} is predominantly found in the regions closest to the star. In that part of the nebula, UV irradiation is high (above 10^4 times the interstellar standard radiation field), and PAH molecules are ionized (Rapacioli et al. 2005; Berné et al. 2007; Pilleri et al. 2012), if not destroyed (Berné & Tielens 2012; Montillaud et al. 2012). One could therefore expect C_{60}^+ to be present in these regions.

Foing & Ehrenfreund (1994) reported evidence of interstellar C_{60}^+ based on the detection of two diffuse interstellar bands (DIBs) at 9577 and 9632 Å, however this identification is still questioned considering that no spectrum of C_{60}^+ could be recorded yet, in conditions appropriate for DIB identification, i.e., in gas phase and at low temperature. The IR spectrum of C_{60}^+ was measured in a rare-gas matrix by Fulara et al. (1993) and was found to exhibit two bands at 7.1 and 7.5 μm . Kern et al. (2012) have performed new spectroscopic measurements and

suggests that the latter band is due to C_{60}^- , whereas the authors attribute a band at 6.4 μm to C_{60}^+ . Moutou et al. (1999) derived upper limits on the abundance of C_{60}^+ in NGC 7023 based on not detecting the 7.1 (and possibly wrongly attributed 7.5 μm) bands. So far, there has been no observational evidence of any 7.1 or 6.4 μm bands in astronomical sources.

Looking carefully at the *Spitzer* data of NGC 7023, we found four emission bands, at 6.4, 7.1, 8.2, and 10.5 μm , which are only present in the regions closest to the star. This also corresponds to a region where C_{60} emission is strong. A natural carrier to explain these bands is C_{60}^+ , and this assertion is supported by spectroscopic arguments that we discuss hereafter.

2. Observations

NGC 7023 was observed with the short-low (SL) and long-low (LL) modules of the InfraRed Spectrograph (IRS, Houck et al. 2004 onboard *Spitzer* (Werner et al. 2004) in spectral mapping mode. The spectral resolution of IRS is $\lambda/\Delta\lambda = 60 - 130$. The slit width (comparable to angular resolution) is 3.6'' for the SL and 10.5'' for the LL modules. Data reduction was performed with the CUBISM software (Smith et al. 2007) and consisted in cube assembling, calibration, flux correction for extended sources and bad pixel removal. From the LL data cube we extracted maps integrated in the H_2 line at 17.0 μm , the PAH band at 16.4 μm and the C_{60} band at 19.0 μm . The maps are presented in Fig. 1 in a fashion similar to Sellgren et al. (2010). From the SL data cube, we extracted two significant spectra corresponding to different regions in the nebula (Fig. 1). The extraction regions were 3x5 pixels (1.6''/pixel) to improve the signal-to-noise ratio. Position 1 corresponds to the cavity of atomic gas between the star and the molecular cloud at an angular distance of 21'' (~ 0.04 pc) from the star HD 200775 ($\alpha=21:01:34.8$, $\delta=+68:10:07.3$).

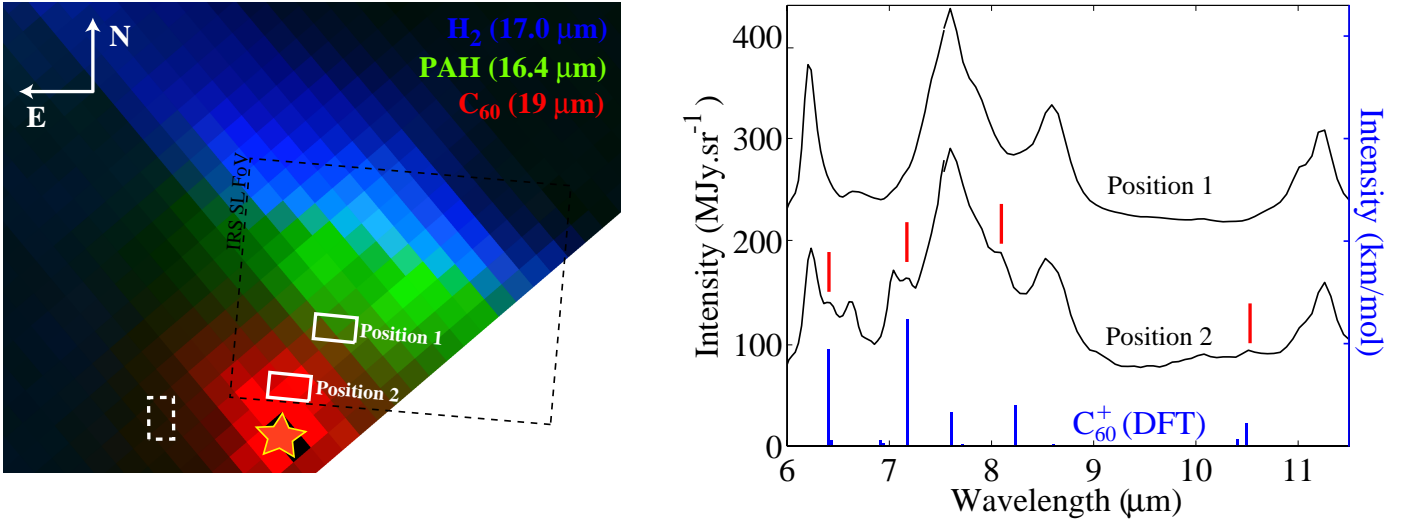


Fig. 1. *Left:* False-color image of the NGC 7023 nebula such as the one presented in Sellgren et al. (2010), obtained from integrating different components in the *Spitzer*-IRS LL spectral cube. Red is the emission integrated in the C_{60} 19 μm band. Green is the emission of the PAH 16.4 μm band. Blue is the emission integrated in the H_2 (0-0) S(0) 17.0 μm band. The white rectangles indicate the regions where the IRS-SL spectra shown in the right panel have been extracted. The black dashed rectangle depicts the IRS-SL field of view. The white dashed rectangle shows the region where Sellgren et al. (2010) extracted their spectrum. *Right:* Spectra at positions 1 and 2 in the image. The spectrum at position 1 has been shifted up and scaled down to allow easier comparison to the spectrum at position 2. Error bars are not shown here but are comparable to the width of the line (see Fig. 2). The red lines indicate the four newly detected bands attributed to C_{60}^+ . The DFT calculated spectrum (with scaled wavelength positions) is shown as a bar graph in blue.

Position 2 ($\alpha=21:01:37.3$, $\delta=+68:09:55.3$) is the closest position to the star in the IRS spectral cube (7.5'', ~ 0.015 pc from HD 200775, see Fig. 1). These two positions correspond to regions where C_{60} emission is strong in the 19.0 μm band (Fig. 1). For both positions the signal-to-noise ratio is very good and ranges between 100 and 200.

3. Observational results

The spectra (Fig. 1) have in common that they are dominated by bands at 6.2, 7.7, 8.6, and 11.2 μm , which are attributed to vibrational modes of PAH molecules (Tielens 2005). In addition to these bands, the spectrum at position 2 shows several bands that are absent in the rest of the nebula. These are at ~ 6.4 , 6.6, 7.0, 7.1, 8.2, and 10.5 μm (Fig. 1). These bands are seen in several pixels of the IRS cube and well above the instrumental errors (Fig. 2). To derive the precise parameters for these bands we fit them using Gaussian profiles (Fig. 1) and splines to subtract the underlying emission due to the wings of PAH bands. The positions, widths, and intensities of the bands are given in Table 1. The 7.0 μm band has been attributed to C_{60} (Sellgren et al. 2010). The 6.6 μm band has recently been attributed to (possible) planar C_{24} (García-Hernández et al. 2011). The 6.4, 7.1, 8.2, and 10.5 μm bands have not been observed or discussed yet. Since HD 200775 is a B star, only low ionization potential atoms should emit in fine structure lines (e.g. [CII], [SIII] etc.), and these species do not have lines in this spectral range, so we exclude contamination by fine structure lines. These four new bands seem spatially correlated, i.e. all of them only appear in the regions closest to the star, which suggests a common carrier. As shown by Sellgren et al. (2010), C_{60} is also found only close to the star. Still, the four new bands only appear in the regions that are closest to the star, while Fig. 1 demonstrates that C_{60} emission is more extended. This suggests that the four new

bands are carried by a species that is a product of the photoprocessing of C_{60} , an obvious carrier being C_{60}^+ . In the following section we provide the spectroscopic arguments that support this observational evidence.

4. Spectroscopy of C_{60}^+

The only IR spectroscopic data of C_{60}^+ has been obtained in rare gas matrices by Fulara et al. (1993) and more recently by Kern et al. (2012). Two bands at 7.1 and 6.4 μm seem definitively attributed to C_{60}^+ , based on these experimental studies.

Theory is another approach to obtaining spectroscopic data, and density functional theory (DFT) in particular has been shown to be effective and accurate for calculations on neutral C_{60} (Chase et al. 1992; Fabian 1996; Iglesias-Groth et al. 2011). However, an additional theoretical problem is that upon ionization C_{60} is known to undergo Jahn–Teller (JT) distortion (Chancey & O’Brien 1997; Bersuker 2006). Neutral C_{60} has I_h symmetry, and is a closed-shell system, and its ground electronic state is totally symmetric and nondegenerate. Upon ionization, the ground electronic state of C_{60}^+ , in the adiabatic approximation, is five-fold degenerate and has h_u symmetry. These electronic states, degenerate at the symmetric configuration, split when the symmetry is broken, and the Jahn–Teller theorem predicts that there must be lower energy extrema, some of which must be minima, at distorted geometries. The closeness of these electronic states means that the adiabatic approximation may break down in this situation. Nevertheless, standard harmonic vibrational spectra can be computed in the adiabatic approximation around the new minima, and they will still be approximately correct if IR-active modes have a negligible component along the directions involved in the Jahn–Teller effect. This is the case for C_{60}^+ , as discussed in Appendix A, where the reader can also

Table 1. Properties of fitted bands for position 2

Position	FWHM	Intensity	Species
μm	μm	$10^{-7} \text{ W m}^{-2} \text{ sr}^{-1}$	Assignment
6.24	0.13	1.02	PAH
6.43	0.09	3.68	C_{60}^+
6.61	0.13	3.41	C_{24}
7.02	0.07	2.92	C_{60}
7.13	0.11	2.82	C_{60}^+
8.10	0.10	0.91	C_{60}^+
8.49	0.14	1.83	C_{60}
8.62	0.28	0.85	PAH
10.53	0.11	0.22	C_{60}^+

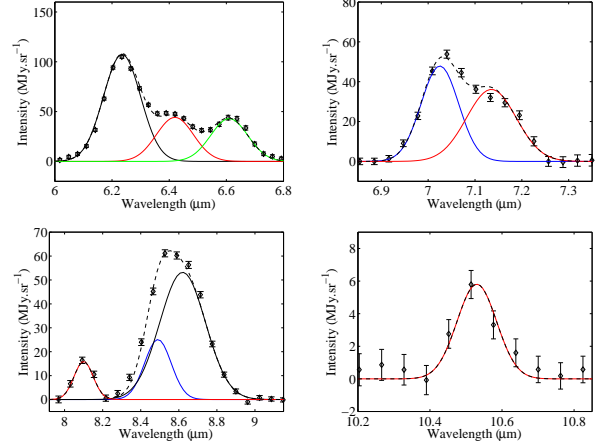
Table 2. Computed IR-active bands of D_{5v} C_{60}^+ . Only IR active modes with an intensity above 0.1 km.mol^{-1} are shown.

Symmetry degeneracy	Unscaled frequency (cm^{-1})	Scaled wavelength* (μm)	Intensity (km.mol^{-1})
E_1 (2)	1607	6.40	94.6
A_2 (1)	1599	6.43	5.5
A_2 (1)	1488	6.91	5.6
E_1 (2)	1482	6.94	2.4
E_1 (2)	1434	7.17	123.8
E_1 (2)	1353	7.60	33.3
E_1 (2)	1333	7.71	1.4
A_2 (1)	1250	8.23	20.0
E_1 (2)	1249	8.23	39.5
E_1 (2)	1196	8.60	1.4
A_2 (1)	989	10.4	6.6
E_1 (2)	981	10.5	22.6
E_1 (2)	795	12.9	2.0
E_1 (2)	778	13.2	6.8
E_1 (2)	763	13.5	0.5
A_2 (1)	592	17.4	3.5
E_1 (2)	588	17.5	0.3
A_2 (1)	553	18.6	19.8
E_1 (2)	412	25.0	12.1
E_1 (2)	364	28.2	5.0
A_2 (1)	361	28.5	0.6

* using an empirical scaling factor $\chi = 0.9725$

find a more detailed description of the Jahn–Teller effect and how it affects our calculations.

We performed our DFT calculations using the hybrid B3LYP exchange–correlation functional and the 4–31g Gaussian basis set. This combination is known to yield reasonably accurate vibrational frequencies, after scaling with an empirical factor χ to account for the overestimation of the frequencies. The relatively small basis set limits the accuracy of band intensities, but based on the thorough tests performed by Galué et al. (2011), we expect that neglecting dynamical JT effects is the leading limitation on vibrational band accuracy even at this level of theory. The distorted geometry of minimum energy was obtained by optimizing with no symmetry constraints, and turned out to have D_{5v} symmetry. This is only very slightly distorted. Such a small change in geometry implies a correspondingly small change in interatomic forces, and it explains the qualitative similarity of the computed spectra of C_{60}^+ and C_{60} . Of course, many more modes are IR-active in distorted C_{60}^+ due to the lowering of symmetry and correspondingly relaxed selection rules. The properties of the most intense IR active bands of C_{60}^+ are given in Table 2.

**Fig. 2.** Fits (dashed line) to the observed bands (diamonds) in position 2. The continuum has been subtracted. Red solid lines denote emission attributed to C_{60}^+ , blue to C_{60} , green to C_{24} , and black to PAHs.

5. C_{60}^+ in NGC 7023

5.1. Identification of C_{60}^+ in NGC 7023

As mentioned in the previous section, it is necessary to correct the calculated frequencies by an empirical scaling factor. In the case of PAHs, this is usually done by comparing the computed frequencies to the ones measured in the laboratory at low temperature in rare gas matrices (see Bauschlicher & Langhoff 1997 for a case-study on PAHs). Therefore we use the IR absorption spectrum of C_{60}^+ that was measured in Ne matrices by Kern et al. (2012) to calibrate our DFT calculations. The two bands definitively attributed to C_{60}^+ by (Kern et al. 2012) are found at 1550 and 1406 cm^{-1} and correspond to the strongest bands, predicted by theory at 1607 and 1434 cm^{-1} . This implies a respective scaling factor of 0.9645 and 0.9805. We adopt an average value $\chi = 0.9725$. The corrected positions are given in Table 2 and the resulting spectrum is shown in Fig. 1. After scaling, the five strongest IR bands fall at wavelengths of 6.40, 7.17, 7.60, 8.23 and $10.50 \mu\text{m}$. Four of these are very close (within 2%) to the positions of the four new bands detected in NGC 7023 (6.43, 7.13, 8.10, $10.53 \mu\text{m}$). The observed match is very good considering that other factors are expected to affect the band positions, in particular band shift due to anharmonic coupling in hot emitting molecules (Joblin et al. 1995). The nondetection of the $7.6 \mu\text{m}$ band in the observations is not surprising, since it is most likely hindered by the strong PAH emission at the same position (Fig. 1). Based on the observational (Sect. 3) and spectroscopic arguments presented in this Letter, we therefore argue that there is strong evidence for the presence of C_{60}^+ in NGC 7023. Further discussion of the relative band intensities would require an emission model. Attempts to build such a model for C_{60} have been reported by Sellgren et al. (2010) and then by Bernard-Salas et al. (2012). However, the authors could not account for the observed relative band intensities. This is likely due to uncertainties in the intrinsic IR band strengths that were obtained by DFT calculations. The same certainly holds for C_{60}^+ for the reasons given in Sect. 4. Still, the detection of C_{60}^+ strongly supports the idea that C_{60} is in the gas phase (Sellgren et al. 2010) and not in solid phase as initially suggested by Cami et al. (2010).

5.2. Abundance

Using a simple energetic consideration, we can derive an estimation of the C₆₀⁺ abundance. We write that C₆₀ and C₆₀⁺ relax in the IR all the energy they absorb in the UV, which is true if IR emission is the only relaxation channel. We can further assume that the UV absorption cross-section of neutral and cationic species are similar, which is the case for PAHs at energies higher than 10 eV (Cecchi-Pestellini et al. 2008). In this case, the ionization fraction of C₆₀ can be directly derived from the integrated IR flux in the C₆₀ and C₆₀⁺ bands. Using the values in Table 1 we find $4.7 \times 10^{-7} \text{ Wm}^{-2} \text{sr}^{-1}$ for C₆₀ and $7.7 \times 10^{-7} \text{ Wm}^{-2} \text{sr}^{-1}$ for C₆₀⁺. However, these values have to be corrected by the emission at longer wavelengths. In the case of C₆₀, we therefore add the emission in the 17.4 and 18.9 μm bands, measured in the IRS2 LL spectrum for position 2 (respectively, 2.6 and $5.2 \times 10^{-7} \text{ Wm}^{-2} \text{sr}^{-1}$). This leads to a total value of $12.5 \times 10^{-7} \text{ Wm}^{-2} \text{sr}^{-1}$ for the total IR flux. In the case of C₆₀⁺, we do not consider emission at longer wavelengths in line with DFT calculations, which predict much weaker bands. Thus, we obtain that the ionization fraction of C₆₀ is 38%. If we consider a maximum abundance of C₆₀ in NGC7023 of 1.7×10^{-4} of the elemental carbon (Berné & Tielens 2012), this implies an abundance of $\sim 1.0 \times 10^{-4}$ of the elemental carbon abundance for C₆₀⁺. This is a factor at least 10 lower than the value derived by Foing & Ehrenfreund (1994) for the diffuse interstellar medium, assuming that C₆₀⁺ is the carrier of the two DIBs at 9577 and 9632 Å. Since the DIB identification is still not firmly established, it is difficult to discuss this discrepancy further.

5.3. Taking the next step, C₆₀⁺ as a tracer of physical conditions

Sellgren et al. (2010) report the detection of the C₆₀ band at 7.0 μm in NGC 7023. In their spectrum, the bands of C₆₀⁺ are not present. Since this spectrum was taken in a region farther away from the star (Fig. 1) this suggests that the C₆₀ emission extends farther away from the star than C₆₀⁺ emission. These relative variations can be attributed to the photochemical evolution of C₆₀ resulting from the competition between ionization by UV photon and recombination with electrons. Assuming one can quantify these two processes, and also have a proper description of the photophysics in these systems, this would allow using the ratio between the IR flux of C₆₀ and C₆₀⁺ as a tracer of local physical conditions. There already exists such an approach using PAH bands (Galliano et al. 2008), but only empirical laws can be used since the PAH population is poorly characterized. Furthermore, information on the C₆₀ and C₆₀⁺ bands is unique for regions of high UV radiation fields in which other molecular tracers may not survive.

6. Conclusion

After studying the mid-IR spectra of the NGC 7023 nebula, we have found spectral signatures at 6.4, 7.1, 8.1, and 10.5 μm , which we attribute to the cationic form of C₆₀ (C₆₀⁺). This is the largest cation known in space so far. C₆₀⁺ has been proposed as a DIB carrier, and our identification supports this proposal. This is also clear evidence for the presence of large carbon molecules in the gas phase in the ISM. The detection of C₆₀⁺ in emission also opens the possibility of using the ratio between the C₆₀ and C₆₀⁺ IR bands as a tracer of physical conditions in interstellar and circumstellar environments. This may prove useful in the

framework of forthcoming infrared missions, such as JWST and SPICA.

Acknowledgements. We acknowledge the French National Program Physique et Chimie du Milieu Interstellaire for its support.

References

- Bauschlicher, C. W. & Langhoff, S. R. 1997, *Spectrochimica Acta Part A: Molecular and Biomolecular Spectroscopy*, 53, 1225
- Bernard-Salas, J., Cami, J., Peeters, E., et al. 2012, *ApJ*, 757, 41
- Berné, O., Joblin, C., Deville, Y., et al. 2007, *Astron. Astrophys.*, 469, 575
- Berné, O. & Tielens, A. G. G. M. 2012, *Proceedings of the National Academy of Science*, 109, 401
- Bersuker, I. C. 2006, *The Jahn–Teller Effect* (Cambridge University Press)
- Cami, J., Bernard-Salas, J., Peeters, E., & Malek, S. E. 2010, *Science*, 329, 1180
- Canton, S. E., Yench, A. J., Kuk, E., et al. 2002, *Physical Review Letters*, 89, 045502
- Cecchi-Pestellini, C., Mallocci, G., Mulas, G., Joblin, C., & Williams, D. A. 2008, *A&A*, 486, L25
- Chancey, C. C. & O’Brien, M. C. M. 1997, *The Jahn–Teller Effect in C₆₀ and Other Icosahedral Complexes* (Princeton University Press)
- Chase, B., Herron, N., & Holler, E. 1992, *The Journal of Physical Chemistry*, 96, 4262
- Fabian, J. 1996, *Phys. Rev. B*, 53, 13864
- Foing, B. H. & Ehrenfreund, P. 1994, *Nature*, 369, 296
- Fulara, J., Jakobi, M., & Maier, J. P. 1993, *Chemical Physics Letters*, 206, 203
- Galliano, F., Madden, S. C., Tielens, A. G. G. M., Peeters, E., & Jones, A. P. 2008, *ApJ*, 679, 310
- Galué, H. A., Rice, C. A., Steill, J. D., & Oomens, J. 2011, *J. Chem. Phys.*, 134, 054310
- García-Hernández, D. A., Iglesias-Groth, S., Acosta-Pulido, J. A., et al. 2011, *ApJ*, 737, L30
- Houck, J. R., Roellig, T. L., van Cleve, J., et al. 2004, *ApJS*, 154, 18
- Iglesias-Groth, S., Cataldo, F., & Manchado, A. 2011, *MNRAS*, 413, 213
- Joblin, C., Boissel, P., Leger, A., D’Hendecourt, L., & Defourneau, D. 1995, *A&A*, 299, 835
- Joblin, C. & Tielens, A. G. G. M., eds. 2011, *EAS Publications Series*, Vol. 46, PAHs and the Universe: A Symposium to Celebrate the 25th Anniversary of the PAH Hypothesis
- Kern, B., Strelnikov, D., Weis, P., Böttcher, A., & Kappes, M. M. 2012, in 67th International Symposium on Molecular Spectroscopy
- Kroto, H. W., Heath, J. R., O’Brien, S. C., Curl, R. F., & Smalley, R. E. 1985, *Nature*, 318, 162
- Montillaud, J., Joblin, C., & Toubanc, D. 2012, submitted to *A&A*
- Moutou, C., Sellgren, K., Verstraete, L., & Léger, A. 1999, *A&A*, 347, 949
- Pillari, P., Montillaud, J., Berné, O., & Joblin, C. 2012, *A&A*, 542, A69
- Rapacioli, M., Joblin, C., & Boissel, P. 2005, *Astron. Astrophys.*, 429, 193
- Saito, M. 2002, *Phys. Rev. B*, 65, 220508
- Sellgren, K., Werner, M. W., Ingalls, J. G., et al. 2010, *Astrophys. J.*, 722, L54
- Smith, H. D. T., Armus, L., Dale, D. A., et al. 2007, *PASP*, 119, 1133
- Tielens, A. G. G. M. 2005, *The Physics and Chemistry of the Interstellar Medium*, ed. Tielens, A. G. G. M.
- Werner, M. W., Roellig, T. L., Low, F. J., et al. 2004, *ApJS*, 154, 1

Appendix A: Details on C₆₀⁺ spectroscopy

Neutral C₆₀ has I_h symmetry, its highest occupied molecular orbital (HOMO) is five-fold degenerate, it has h_u symmetry and is fully occupied, resulting in a closed-shell ground state that is totally symmetric and nondegenerate. Upon ionization, the hole in the h_u HOMO yields a five-fold degenerate h_u overall electronic state. This undergoes spontaneous symmetry-breaking due to the Jahn–Teller (JT) effect (Chancey & O’Brien 1997; Bersuker 2006). The degeneracy of the electronic state is lifted by distorting the molecule to a lower symmetry along some of its normal modes, which are determined by symmetry and called JT-active. For C₆₀⁺, JT-active modes are those of H_g , G_g , and A_g symmetry. The A_g modes only shift the total energy, without reducing symmetry. The H_g , G_g modes instead break the I_h symmetry, and produce a multisheet adiabatic potential energy surface, with a

conical intersection in the symmetric geometry and extrema in configurations of D_{5v} and D_{3v} lowered symmetry. DFT predicts that the D_{5v} geometries should be the absolute minima, with the D_{3v} ones being shallow transition states (Saito 2002). However, high-resolution photo-electron spectroscopy seems to hint that the D_{3v} geometry could be the real minimum (Canton et al. 2002). When JT-distorted minima are deep with respect to vibrational energy (*static* JT-effect), the adiabatic approximation holds in its vicinity, and standard harmonic vibrational analysis is applicable. Conversely, if equivalent minima are separated by negligible potential barriers, the molecule can tunnel among equivalent minima, mixing the near-degenerate electronic states (*dynamic* JT-effect), and the adiabatic approximation is not applicable. The resulting vibronic states recover the full initial symmetry of the problem. In this case, a much more complex calculation, dropping the adiabatic approximation, is needed for accurate results. A comparable, but much simpler case of dynamical JT effect is the cation of corannulene, $C_{20}H_{10}^+$, which can be regarded as a fragment of C_{60} with peripheral bonds saturated by H atoms. This was studied by Galué et al. (2011), who compared experimental infrared, multiphoton dissociation (IRMPD) spectra with a plain DFT harmonic vibrational analysis at the distorted geometry of minimum energy. This was expected to be the worst possible comparison, since in IRMPD experiments, vibrational energy is increased until the dissociation threshold is reached. This corresponds to energy values that are much higher than all barriers among equivalent minima, thereby maximizing dynamical JT effects. Despite this, the experimental and theoretical spectra do qualitatively agree, allowing for accurate band identification. Bands that are most significantly mispredicted, in position and intensity (but still identifiable in the laboratory spectrum), are those whose normal modes imply displacement along JT-active modes, i. e. those that move the molecule from a minimum in the direction of another one, or to the conical intersection.

In the light of this, we did a similar analysis for C_{60}^+ , finding the distorted geometry of minimum energy and computing harmonic vibrational spectra there, thereby neglecting dynamical JT effects. We performed DFT calculations using both the Gaussian version 03.d2 and NWChem version 6.1 codes, and obtained very nearly identical results. Optimization led to the D_{5v} geometry. We also optimized the geometry of C_{60}^+ with the constraint of I_h symmetry, obtaining a JT stabilization energy of ~ 70 meV, which is consistent with previous calculations (Saito 2002). The D_{5v} distorted geometry, when compared with the symmetric one, appears to be distorted almost exclusively along normal modes of H_g symmetry, with changes in bond lengths of a few mÅ and bond angles by less than a degree (maximum).